Delft University of Technology

Semi-analytical model for the prediction of the Wilson point for homogeneously condensing steam flows

Azzini, Lucia; Pini, Matteo; Colonna, Piero

Important note
To cite this publication, please use the final published version (if applicable).
Please check the document version above.

Semi-analytical model for the prediction of the Wilson point for homogeneously condensing steam flows

L. Azzini, M. Pini*, P. Colonna

Propulsion and Power, Delft University of Technology, Kluyverweg, 1, Delft 2628HS, The Netherlands

ARTICLE INFO

ABSTRACT

An investigation on non-equilibrium condensing steam flow is conducted to attain a semi-analytical model for the prediction of the Wilson point up to the critical point. The database for the analysis includes experimental observations in various nozzles and conditions (ranging from 20 to 150 bar) taken from the literature as well as additional data at lower and higher reduced pressures, generated by means of a calibrated quasi-1D model based on the method of moments.

The simplified model is based on a reformulation of the Wilson point in terms of activation time, defined as the temporal interval between the instant at which the flow is at saturation conditions and the inception stable of condensation. This allows to incorporate the dependency of the Wilson point on the cooling rate and dew-point temperature, which are found the key parameters affecting the delay of condensation.

The accuracy of the approach is proved by predicting the degree of subcooling on four different test cases, with deviations against experiments in the range of $1 - 10\%$. As demonstrated, the same approach can be exploited to design nozzles free of condensation.

1. Introduction

Condensing flows are nowadays encountered in many different fields of science and engineering. For example, several current studies treat atmospheric condensation phenomena, as part of improved climate models (Kulmala et al., 2004). Condensation phenomena are also exploited in biotechnology (Bruno and Ely, 1991) and for biomedical purposes: as described in Ref. Sheeran et al. (2016), micro-droplets are created as part of an ultrasonic medical treatment.

Furthermore, the impact of two-phase flows is significant in multiple engineering applications. Condensation is sometimes provoked within heat exchangers in order to enhance heat transfer (Leipertz and Fröba, 2008). Vapour–liquid transition occurs in steam turbines (Guo et al., 2007), expanders and water separation processes for the oil and gas industry (IJzermans et al., 2007), and moist-air nozzles flows for transonic expansions in aero-engines (Hamidi and Kermani, 2015).

The inception of stable condensation in high-speed flows usually occurs at temperatures which are several degrees lower than the saturation temperature T_{sat}, in correspondence with the so called Wilson point (Gyarmathy, 1962). In these conditions, namely P_w, T_w, unstable liquid clusters reach the critical radius required to overcome the Gibbs free-energy barrier, and evolve into stable liquid droplets (McDonald, 1974).

The difference $T_{\text{sat}} - T_w$ is termed degree of subcooling, and its prediction is of paramount importance in the fluid dynamic design of machinery or devices in general, as this quantity is directly associated to the thermodynamic wetness losses due to the heat transfer between the two phases (Gyarmathy, 2005; Young, 1984).

Many authors attempted to relate the degree of subcooling to macroscopic flow quantities like (i) the dew-point temperature T_{sat} and (ii) the expansion rate $\dot{P}$ (Gyarmathy, 2005) defined as

$$\dot{P} = \frac{1}{P_0} \frac{\partial P}{\partial t},\tag{1}$$

in which P_0 is the total pressure, P the local vapour pressure and t the time. Detailed investigations were conducted on steam supersonic expansions from both the experimental (Gyarmathy, 2005; Yellott, 1934; Bakhtar and Zidi, 1989; Gyarmathy, 1963) and the numerical (Bakhtar and Zidi, 1990; White, 2003; Gerber and Kermani, 2004; Dykas and Wróblewski, 2012) points of view to gain knowledge on the effect of $\dot{P}$ and T_{sat} on the Wilson temperature. Gyarmathy (1962) showed that the expansion rate is one of the main parameters affecting the inception of stable condensation. In particular, the higher is $\dot{P}$ the lower can be T_w. However, as stated by Ryzhov et al. (1989), such dependence cannot be quantified satisfactorily for a wide range of operating conditions, due to the contradictory results of the different data sets available. For some of

---

the measurements the impact of $\dot{P}$ on T_w is not clearly visible, arguably due to the large uncertainties affecting the experiments. Moreover, the parameter $\dot{P}$ is expected to have a limited influence on the condensation onset at high reduced temperatures (Bier et al., 1990). This would comply with the fact that in correspondence to the critical point the relation

$$T_w = T_{cr} \qquad (2)$$

must hold, regardless of the expansion rate. In the proximity of the critical point, the spinodal curve is increasingly closer to the saturation line, thus the Wilson temperature is constrained to also approach T_{sat}. Moreover, the surface tension vanishes at the critical point, reducing the energy barrier required to form a stable nucleus. These theoretical considerations have never been proved experimentally and, at present, no quantitative characterization of the Wilson point close to the critical point is known.

Simplified numerical models for the prediction of the Wilson point are reported in Refs. Young (1984), Dobbins (1983), Ding et al. (2015) and Huang and Young (1996). However, despite the numerous studies on the subject, there is still no clear understanding on how the location of the Wilson point, thus the degree of subcooling, is affected by the thermal and fluid dynamics characteristics of the vapour undergoing homogeneous condensation.

This work aims at addressing these issues by theoretically and numerically investigating the onset of condensation for different types of nozzle geometries and operating conditions. At first, the determining parameters driving the process of condensation are recognized by using an analytical approach based on the classical nucleation theory. Then, a systematic analysis on supersonic flow expansions is conducted by means of a quasi-1D numerical model to calculate the degree of subcooling for each case. By introducing a new dimensionless quantity, referred to as *Wilson number Wi*, a simplified and computationally affordable method to estimate the Wilson temperature T_w is derived. This enables to gain physical insights on the conditions affecting the Wilson point, and to predict its trend in the vicinity of the critical point. Eventually, the potential of the method for design purposes is illustrated. Given the large number of experiments on condensing steam flows, the proposed semi-analytical model has been developed based on these data, but it can be easily extended to any other condensing fluid.

The paper is structured as follows: the second section describes the adopted numerical methodology. The third section reports the conceptual steps followed to obtain a correlation for the estimation of T_w. The last section documents the application of the proposed approach to generic nozzle expansions.

2. Numerical methodology

The numerical calculations are conducted with an Eulerian–Eulerian quasi-1D model constituted by (i) the three conservation laws for the continuum phase and (ii) two additional transport equations for the droplet properties (number and liquid title). These relations are formulated by exploiting the method of moments described in Put (2003). As demonstrated in White (2003), this approach proved to be computationally more efficient and numerically more robust than other methods. The interested reader can find a detailed description of the model in Azzini et al. (2016). The solution of the equations giving the moments requires two closure relations for the nucleation rate J_s and the growth rate G_s. In this study, the non-isothermal nucleation rate reported in Bakhtar et al. (2005) and the growth rate in Giordano et al. (2010) have been adopted.

The dispersed phase is assumed to be in mechanical and kinematic equilibrium with the vapour, i.e., no-slip between the two phases. Additionally, the liquid phase temperature is evaluated by using a simplified capillarity model (Dykas and Wróblewski, 2012). The thermo-physical properties of the vapour phase are estimated with a thermodynamic model based on the iPRSV equation of state (van der

Stelt et al., 2012; Colonna and der Stelt, 2004). The use of a complex thermodynamic model allows to account for the non-ideal thermodynamic behaviour of the flow at high reduced pressure. The droplet properties are calculated with the IF-97 model (Wagner et al., 2008). Finally, the surface tension σ_s is estimated using the model described in Vargaftik et al. (1983).

2.1. Model calibration

As observed in Refs. Giordano et al. (2010), Lai and Kadambi (1990) and Halama and Fort (2012), the adoption of J_s, G_s, σ_s in the classical form (Azzini et al., 2016) leads to an exceedingly high Wilson pressure P_w, deviating from the experimental value by a large amount. Part of this difference is caused by the intrinsic limitations of the classical nucleation theory. It was established that the location of the nucleation onset is particularly sensitive to the steam heat capacity ratio γ (Bakhtar et al., 2005). Especially when approaching high-pressures, small variations of this parameter can increase the discrepancy between the theoretical solution and the measurements. Moreover, the surface tension is usually affected by considerable uncertainties, and existing correlations do not take into account any droplet curvature effects (Lai and Kadambi, 1990). As a consequence, due to the exponential dependence of J_s on σ_s, the theoretical Wilson pressure P_w and the droplet properties are far from the experimental data.

Therefore, empirical coefficients are customarily introduced (Bakhtar et al., 2005; Lai and Kadambi, 1990) to correct the parameters σ_s, J_s, G_s in order to reach a better accuracy. Following Azzini and Pini (2017), σ_s, J_s, G_s are then multiplied by an empirical factor, yielding to

$$\sigma = r_\sigma \sigma_s, \qquad J = r_J J_s, \qquad G = r_G G_s, \qquad (3)$$

in which the values r_σ, r_J, r_G are calibrated to achieve the best fit with the measurements. The database for the calibration includes experimental measurements on four different nozzle profiles reported in Ref. Gyarmathy (2005). The nozzle geometries are also here referred to as *2B, 4B, 5B, 6B*, and the experiments cover a wide range of pressures (total pressure P_0 from 20.82 bar to 149.74 bar).

For each test, the three corrections r_σ, r_J, r_G have been determined empirically, in order to match the experimental observations in terms of Wilson pressure P_w, droplet average radius $\overline{R}_w$ and number N_w. For some of the tests, no uncertainty interval on the measurements is reported. In all cases in which uncertainty is unknown, the nominal values were used for the calibration. These cases are marked with the superscript $-*-$ hereinafter. Appendix A reports the procedure to obtain the correction factors for expansion test *21As** as an exemplary case. Appendix B reports the calibration factors obtained from all available experiments. Fig. 1 depicts the Wilson point in the *P-T* chart obtained from the calculations.

Correlation of r_σ, r_J, r_G for nozzle 2B. Initially, in order to limit the number of parameters affecting the calibration, only the data of a single nozzle profile, i.e., *2B*, were considered. Fig. 2 shows the values of r_σ, r_J, r_G as a function of the Wilson pressure P_w.

Several fitting functions, i.e. logarithmic, exponential, polynomial, power law, have been tested in order to find the best fit for the values of the calibration parameters according to the L2 norm. The best fitting function is given by

$$r_{\sigma, J, G} = \frac{P_w - a}{c P_w - b} + 1 - \frac{a}{b}, \qquad (4)$$

in which the pressure P_w is in bar. In cases in which the fitting leads to a and b having very similar values, a and b are set equal in order to avoid numerical problems.

The coefficients a, b, c are reported in Table 1. Note that, as the low-pressure simulations documented in Refs. Gerber and Kermani (2004),
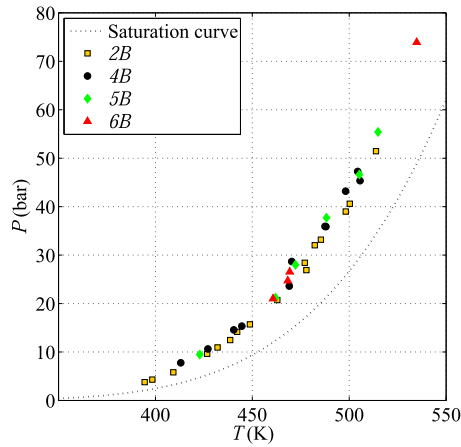
Fig. 1. Wilson point on the *P-T* chart obtained from the simulations, see Table B.6 and B.7.
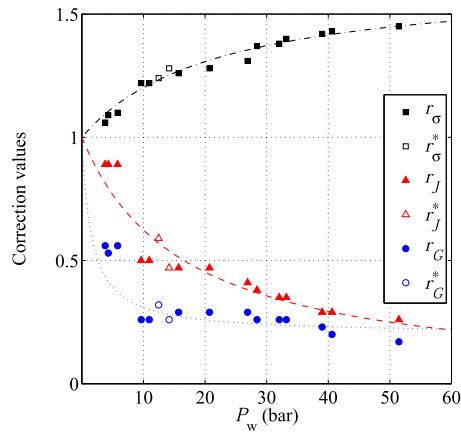

Fig. 2. Values of r_σ, r_G, r_J for nozzle *2B* and interpolation function according to Eq. (4) (coefficients reported in Table 1).

Table 1
Correlation between r_σ, r_J, r_G and P_w: hyperbola coefficients according to Eq. (4) for nozzle *2B*.

	a(bar)	b(bar)	c
r_σ	−13.3057	−13.3057	0.6086
r_J	−23.4400	−6.9865	0.4241
r_G	−7.7696	−7.7696	4.9642

Azzini et al. (2016) and Giordano et al. (2010) well correlate with the measurements, the curve in Eq. (4) is constrained to pass through the point (0, 1). In other words, it is assumed that low P_w expansions can be modelled with values of r_σ, r_J, r_G equal to one.

Dependence of r_σ, r_J, r_G on the expansion rate. The analysis was repeated for the data of all the four nozzle geometries in order to account for different expansion rates. Figs. 3–5 display the values for r_σ, r_J, r_G as a function of P_w.

Remarkably, r_σ and r_J appear to be independent from $\dot{P}$. The fitting functions based on Eq. (4) are displayed in Figs. 3 and 4. The coefficients a, b, c are reported in Table 2.

As can be noted, Fig. 5 shows that r_G values related to high cooling rate are much closer to one compared to the others. Therefore, if the expansion rate of the nozzle is high, the correction of the growth rate G must be correspondingly large. As a consequence, the r_G fitting function must be dependent on $\dot{P}$. However, it can be observed from Appendix A that r_G mainly affects the radius and the droplet number, whereas the
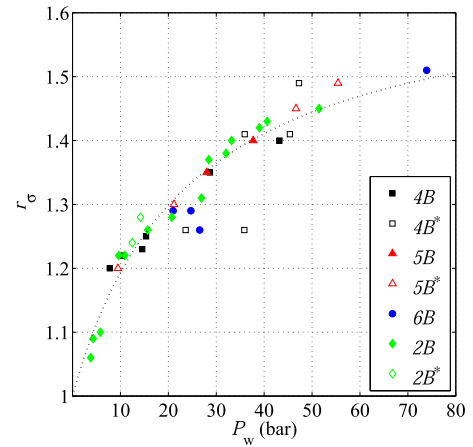

Fig. 3. Values of r_σ for nozzles *2B, 4B, 5B, 6B* and interpolation function according to Eq. (4) (coefficients reported in Table 2).

Table 2
Correlation between r_σ, r_J, r_G and P_w: hyperbola coefficients according to Eq. (4) for nozzles *2B, 4B, 5B, 6B*.

Parameter	Valid for nozzles	a(bar)	b(bar)	c
r_σ	all nozzles	−14.5208	−14.5208	0.6031
r_J	all nozzles	−34.7273	−22.5671	1.6392
r_G	nozzle 2B	−7.7696	−7.7696	4.9642
	nozzle 4B	−11.4766	−9.1298	2.0838
	nozzle 5B	−2.3322	−2.3322	2.5498
	nozzle 6B	−5.7402	−5.7402	1.4348

Fig. 4. Values of r_J for nozzles *2B, 4B, 5B, 6B* and interpolation function according to Eq. (4) (coefficients reported in Table 2).

influence on the Wilson point is rather low.

2.2. Comparison with literature

A summary of the simulations can be found in Tables B.6 and B.7, while the corresponding Wilson points are depicted in Fig. 6.

In order to verify the compatibility of the simulations with a wider range of measurements, the results were first compared to the data collected in the test cases of Ryzhov et al. (1989). Fig. 6 reports the values of T_w as a function of the temperature $T_{sat}(s_0)$, i.e., the saturation temperature in correspondence with the entropy

$$s_0 = s(P_0, T_0), \tag{5}$$

where P_0, T_0 are the total inlet conditions of the flow. The correlation coefficient R^2 associated with the simulation results and the
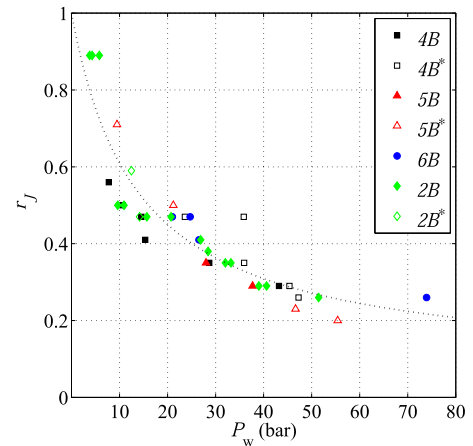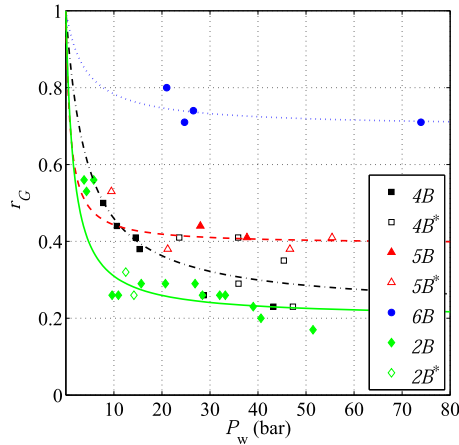
Fig. 5. Values of r_G for nozzles *2B, 4B, 5B, 6B* and interpolation function according to Eq. (4) (coefficients reported in Table 2).
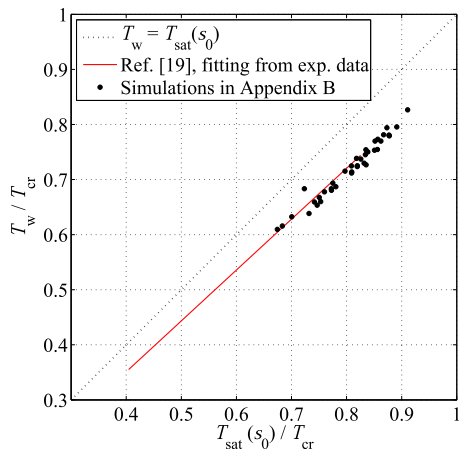

Fig. 6. Wilson temperature T_w as a function of the saturation temperature $T_{sat}(s_0)$: comparison between the present work and the results in Ryzhov et al. (1989).
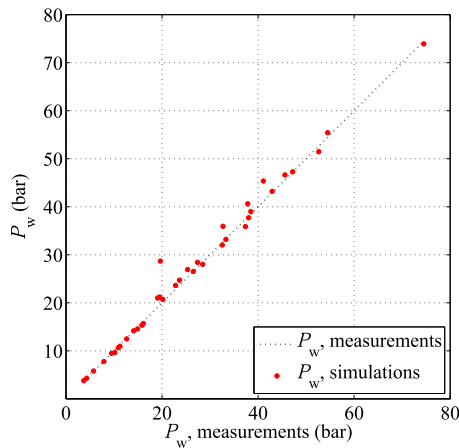

Fig. 7. Comparison between the condensation pressure evaluated through the numerical model and the experimental measurements in Ryzhov et al. (1989).

experimental data is 0.997 (Fig. 7), which is deemed satisfactory.

Note that Fig. 6 shows the linear trend as reported in Ryzhov et al. (1989). However, such trend is misleading, and the dependence of T_w from the rate of the expansion is commonly accepted.

3. Parameters affecting the condensation onset

Physical evidence and more recent studies suggest that the difference $T_{sat}(s_0) - T_w$ is intimately related to the expansion rate (Gyarmathy, 2005). Ideally, for $\dot{P}$ values approaching 0 the fluid must condense at saturation conditions. Formally, the determining parameters influencing the condensation onset can be retrieved by working out the classical nucleation theory. Let be α the liquid volume, defined as

$$\alpha = \frac{4}{3}\pi N \overline{R}^3, \tag{6}$$

i.e., the volume occupied by a number N of spherical droplets with an average radius $\overline{R}$. The time derivative of α can thus be expressed as

$$\dot{\alpha} = \frac{4}{3}\pi \overline{R}^2 (R\dot{N} + 3N\dot{\overline{R}}) = \dot{\alpha}(\dot{N}, \dot{\overline{R}}, \overline{R}, N) \simeq \dot{\alpha}(J, G, \overline{R}, N), \tag{7}$$

in which the nucleation and the growth rate J and G are used to model the two derivatives $\dot{N}$, $\dot{\overline{R}}$.

The four terms J, G, $\overline{R}$, N are now analysed separately. The nucleation rate adopted in the present study has the form

$$J = \frac{1}{1+\theta}\frac{\rho_v}{\rho_l}\sqrt{\frac{2\sigma}{\pi m^3}}\exp\left(-\frac{4\pi\overline{R}_*^2\sigma}{3KT_v}\right), \tag{8}$$

where

$$\theta = 2\frac{\gamma-1}{\gamma+1}\frac{h_v-h_l}{\mathscr{R}T_v}\left(\frac{h_v-h_l}{\mathscr{R}T_v}-0.5\right), \tag{9}$$

$$\overline{R}_* = \frac{2\sigma}{\rho_l\Delta\mathscr{G}}. \tag{10}$$

In Eq. (10), σ is the surface tension, m is the molecular mass, K is the Boltzmann constant, $\rho_{v,\,l}$ and $h_{v,\,l}$ are the densities and the specific enthalpies of the vapour and the liquid phase, $\Delta\mathscr{G}$ is the free Gibbs energy variation of the steam and $\mathscr{R}$ is the gas constant.

Moreover, it is assumed that the liquid and the vapour are in mechanical equilibrium, and that the temperature of the droplets depends on the vapour temperature through a capillary model (Azzini et al., 2016). It can be concluded that the liquid properties are a function of T_v, P_v and $\overline{R}$. From Eqs. (8)–(10) and the last consideration it can be inferred that

$$J = J(P_v, T_v, \overline{R}, m, \gamma). \tag{11}$$

The growth rate G is now examined. The relation adopted is in the form

$$G = \frac{\kappa_v(T_{sat}(P_v)-T_v)\left(1-\frac{\overline{R}_*}{\overline{R}}\right)}{\rho_l(h_v-h_l)\left(1.89+\overline{R}-1.89\nu\frac{\lambda_v}{Pr_v}\right)}, \tag{12}$$

in which λ_v is given by

$$\lambda_v = \frac{1.5\mu_v\sqrt{\mathscr{R}T_v}}{P_v}, \tag{13}$$

κ_v and μ_v are the thermal conductivity and viscosity of the vapour phase and ν is defined as

$$\nu = \frac{\mathscr{R}T_{sat}(P_v)}{h_v-h_l}\left[0.5-\frac{1}{4}\frac{\gamma+1}{\gamma-1}\frac{\mathscr{R}T_{sat}(P_v)}{h_v-h_l}\right]. \tag{14}$$

It follows that

$$G = G(T_v, P_v, \overline{R}, m, \gamma), \tag{15}$$

and, by replacing G with the temporal derivative of the radius $\dot{\overline{R}}$, we have that

$$\dot{\overline{R}} = \dot{\overline{R}}(T_v, P_v, m, \gamma). \tag{16}$$

Substituting Eqs. (11) and (16) in Eq. (7) yields

$$\dot{\alpha} = \dot{\alpha}(T_v, P_v, N, m, \gamma),\tag{17}$$

or, equivalently, by inverting the relation,

$$T_v = T_v(\dot{\alpha}, P_v, N, m, \gamma).\tag{18}$$

The term N is now considered. By applying the conservation law for the moment of order 0 (Azzini et al., 2016), it can be noted that N is a function of the density mixture ρ_m, the velocity v of the flow, the cross sectional area variation along the nozzle $\frac{dA}{dx}$, the critical radius $\overline{R}_*$ and J. In mathematical terms, this results in

$$N = N\left(\rho_m, v, \frac{dA}{dx}, \overline{R}_*, J\right) = N\left(\rho_v, \rho_l, \alpha, v, \frac{dA}{dx}, \overline{R}_*, J\right)$$
$$= N\left(T_v, P_v, \alpha, v, \frac{dA}{dx}, m, \gamma\right).\tag{19}$$

Finally, the conservation law for the moment of order 3 states that

$$\alpha = \alpha\left(\rho_m, \rho_l, v, \frac{dA}{dx}, N, J, G, \overline{R}, \overline{R}_*\right) = \alpha\left(T_v, P_v, v, \frac{dA}{dx}, N, m, \gamma\right).\tag{20}$$

As a consequence, the combination of Eqs. (18)–(20) leads to

$$T_v = T_v\left(P_v, v, \frac{dA}{dx}, m, \gamma\right).\tag{21}$$

The temperature $T_{sat}(s_0)$ is now introduced. The bulk of a nozzle flow before inception of condensation can be assumed to be isentropic. The mass and energy balances between a generic state characterized by T_v and the saturation state $T_{sat}(s_0)$ along the expansion can be written as

$$\begin{cases} \rho_v(T_v, s_0)A_v v_v = \rho_{sat}(T_{sat}, s_0)A_{sat} v_{sat} \\ h_v(T_v, s_0) + \frac{1}{2}v_v^2 = h_{sat}(T_{sat}, s_0) + \frac{1}{2}v_{sat}^2 \end{cases}.\tag{22}$$

Given the nozzle geometry and the value $T_{sat}(s_0)$, system (22) determines the velocities v_v, v_{sat}, thus the steam mass flow $\dot{m}_{flow}$ and the total enthalpy h_0. From Eqs. (21) and (22) it can be deduced that

$$T_v = T_v\left(\frac{dA}{dx}, T_{sat}(s_0), m, \gamma\right),\tag{23}$$

as the velocity v as well as the vapour pressure P_v can be easily retrieved through T_v, $\dot{m}_{flow}$, h_0 and the nozzle area distribution.

Finally, $\frac{dA}{dx}$ can be expressed as a function of $\frac{dT_v}{dx}$, i.e., the temperature gradient along the nozzle. The mass balance for an isentropic expansion is
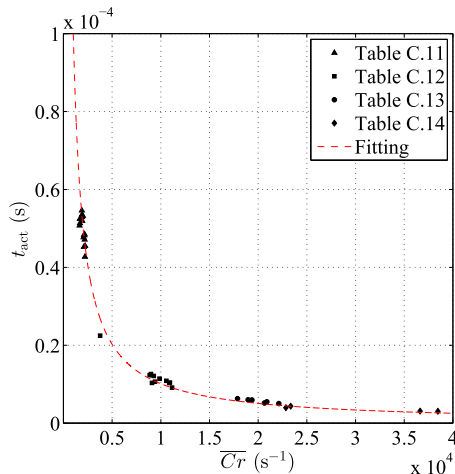

Fig. 8. Activation time as a function of the cooling rate for the simulations in Tables C.11–C.14. Fitting with $Wi = 0.1012$, constant.

$$\frac{d\rho_v}{\rho_v} - \frac{dh_v}{v_v^2} + \frac{dA}{A} = 0.\tag{24}$$

At each value dT_v corresponds a unique variation in density $d\rho_v$ and in specific enthalpy dh_v along the same isentrope. Thus, it is possible to write

$$\frac{d\rho_v(dT_v, s_0)}{\rho_v} - \frac{dh_v(dT_v, s_0)}{v_v^2} + \frac{dA}{A} = 0.\tag{25}$$

The term dA is then related to dT_v and s_0. As a result, if the temperature is the temperature of the Wilson point, Eq. (21) becomes

$$T_w = T_w(dT_v, T_{sat}(s_0), m, \gamma),\tag{26}$$

where dTv can be expressed through the time derivative $\frac{\partial T}{\partial t}$. From Eq. (26) it follows that the Wilson point T_w is primarily a function of (i) the temperature $T_{sat}(s_0)$ (ii) the temperature variation along the nozzle and (iii) the fluid under scrutiny. The proposed analytical derivation is not a general proof, as it is valid only for the stated specific set of equations, closure relations and assumptions. A more formal mathematical demonstration, which led to the same conclusions, is treated in Ryzhov et al. (1989). The analytical closure of Eq. (26) is discussed in Section 3.1.

3.1. Numerical determination of the Wilson point

The key-idea for the calculation of the Wilson temperature is the fact that there exists a correlation between the average cooling rate $\overline{Cr}$ to which the subcooled vapour is subjected and the time elapsing from the instant in which saturated conditions are achieved until the onset of stable condensation. This time interval, defined as *activation time* t_{act}, allows to cast the temperature difference $T_{sat}(s_0) - T_w$ in dimensionless form as

$$\frac{T_{sat}(s_0) - T_w}{T_{cr}} = \overline{Cr} \cdot t_{act},\tag{27}$$

where $\overline{Cr}$ is the average cooling rate in s^{-1} of the subcooled steam.[1] Hereinafter the left term of Eq. (27) is referred to as *Wilson number Wi*. Thus, from the physical point of view Wi can be seen as the dimensionless vapour subcooling along an isentrope. From the same relation it follows that

$$T_w \stackrel{def}{=} T_{sat}(s_0) - T_{cr} Wi(T_{sat}(s_0), t_{act}).\tag{28}$$

Appendix C reports the activation time and the cooling rate for all the simulations, whereas Fig. 8 depicts t_{act} as a function of $\overline{Cr}$. Notably, the activation time in Fig. 8 can be well approximated by a rectangular hyperbola characterized by Wi equal to 0.1012. Only for the considered range of temperatures and $\overline{Cr}$, the Wilson point is nearly independent from the cooling rate and thermodynamic conditions of the fluid, as already highlighted in Fig. 6.

The dependence of t_{act} on $\overline{Cr}$, namely $t_{act} = f(\overline{Cr}) = Wi/\overline{Cr}$, can be interpreted starting from what is commonly known about the physical mechanism of condensation. All the states for which $t > f(\overline{Cr})$ are characterized by the presence of condensate, whereas for time values $t < f(\overline{Cr})$ stable nucleation does not occur.

Therefore, by conventionally defining $t = 0$ s the time instant at which the fluid is at saturation conditions, t_{act} can be viewed as the temporal limit for which stable droplet formation is inhibited. In physical terms, for each value $\overline{Cr}$, the steam remains subcooled for a finite time, after which stable condensation is triggered.

The activation time t_{act} is a characteristic of the condensation process , and as such it depends on the same parameters determining T_w. Section 3.1.1 illustrates the quantitative dependence of cooling rate and dew point temperature on t_{act}.

---

[1] The local cooling rate Cr is defined as $\frac{1}{T_{cr}}\frac{\partial T}{\partial t}$

Table 3
Synthetic simulations characterized by low $\overline{Cr}$ values: nozzle profile and total inlet conditions.

Simulation	Profile	Stretch[a]	P_0(bar)	T_0(K)
M	Moore et al. (1973)	1	0.250	358.0
Mx10	Moore et al. (1973)	10	0.250	358.0
Mx25	Moore et al. (1973)	25	0.250	358.0
Mx1e5	Moore et al. (1973)	1e5	0.281	380.2[b]
Mx1e10	Moore et al. (1973)	1e10	0.281	380.2[b]

[a] Due to the lack of data for low $\overline{Cr}$ values, synthetic data were generated by stretching the nozzle to further reduce the cooling rate.

[b] Total conditions are imposed such that the flow enters at sonic conditions in the two-phase region, at the same temperature as for the test *M*.
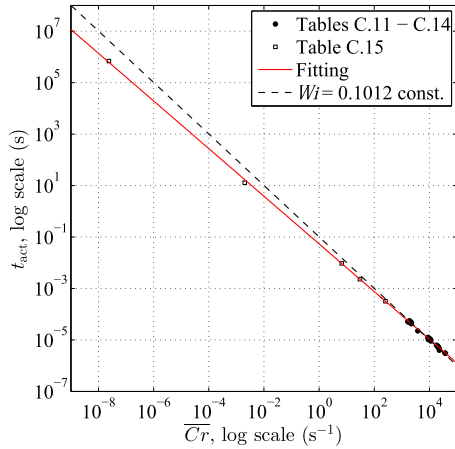

Fig. 9. Activation time as a function of the cooling rate for the simulations in Tables C.11–C.15.

Fig. 10. Wilson number Wi as a function of $\overline{Cr}$ according to Eq. (30).

Fig. 11. *T-s* chart reporting (i) saturation curve, (ii) spinodal curve and (iii) Wilson point as in Eq. (30) for $\overline{Cr}$ values of 1, 100 and 10 000 s^{-1}.

3.1.1. Dependence of the Wilson number on the cooling rate $\overline{Cr}$

To explicitly assess the impact of the cooling rate on Wi, three further calculations were carried out for different values of $\overline{Cr}$. Additionally, two expansion simulations with $\overline{Cr}$ approaching 0, namely *Mx1e5* and *Mx1e10*, were also performed, to prove that at very low $\overline{Cr}$ the subcooling reduces considerably, and the temperature T_w is almost equal to $T_{sat}(s_0)$. Table 3 reports the nozzle profiles and the total inlet conditions for these test cases, whereas Tables B.10 and C.15 report the Wilson point and the activation time.

Fig. 9 displays the activation time as a function of the cooling rate for all the test considered cases. The fitting led to

$$t_{act} = k_1 \overline{Cr}^{-k_2}, \qquad k_1 = 0.0539, \qquad k_2 = 0.9257. \tag{29}$$

It is pointed out that a simple quasi-1D model is not sufficiently reliable for an accurate prediction of the flow motion field for tests *Mx1e5* and *Mx1e10*, due to the high stretch factor adopted. However, the results obtained are not visibly influencing the trend in Fig. 9.[2]

From the definition of Wi and Eq. (29) it follows that

$$Wi = t_{act}\overline{Cr} = k_1 \overline{Cr}^{1-k_2}. \tag{30}$$

For specified $T_{sat}(s_0)$, the Wilson point is weakly dependent on the cooling rate ($k_2 \approx 1$), suggesting that very large cooling rates $\overline{Cr}$ variations are necessary to obtain appreciable changes of the Wilson temperature, see Fig. 10. In practice, the range of $\overline{Cr}$ values considered in Fig. 10 comprises all the Wilson states that can be typically encountered in steam expansion processes. Fig. 11 reports a *T-s* diagram indicating the locus of the Wilson points evaluated according to Eq. (30) for $\overline{Cr}$ values of 1, 100 and 10 000 s^{-1}. The dimensional values
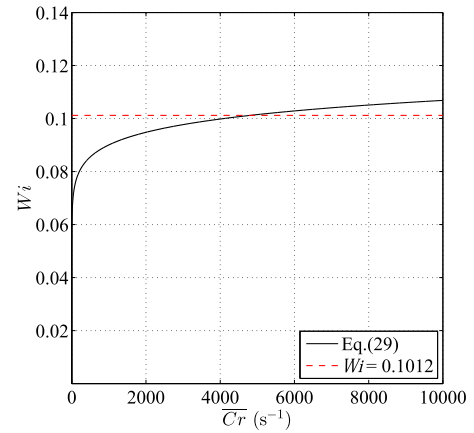
of the cooling rates are therefore $6.47e2$, $6.47e4$, $6.47e6$ K/s.

Finally, it can be observed that for $\overline{Cr}$ values ideally approaching 0 Wi vanishes according to Eq. (30). As a consequence, the Wilson temperature coincides with the saturation temperature, in agreement with the definition of thermodynamic equilibrium. From a mathematical point of view, for $\overline{Cr}$ approaching 0, t_{act} must tend to $+\infty$, see Eq. (29): the physical time required to reach almost zero subcooling, i.e. $Wi \rightarrow 0$, with a cooling rate approaching 0 is an indeterminate form 0/0.

3.1.2. Dependence of the Wilson number on $T_{sat}(s_0)$

The curves obtained with Eq. (29) predicts non-physical states in the vicinity of critical point, since these predicted states are unstable, see Fig. 11. Thus, Eq. (30) must be modified in order to i) maintain the same dependence on $\overline{Cr}$ observed for low temperatures and ii) fulfil the condition (2) in correspondence of T_{cr}.

Therefore, synthetic data in the vicinity of the critical point and instrumental to this purpose were generated. Two simulations with total reduced inlet conditions equal to (a) $P_{0,r} = 0.70$, $T_{0,r} = 0.96$ and (b) $P_{0,r} = 0.81$, $T_{0,r} = 0.98$ were carried out for each of the nozzle profiles reported in Gyarmathy (2005). It was not possible to perform simulations with inlet total conditions with $P_{0,r} > 0.81$ because the calculation of metastable states fails due to numerical singularities. For the sake of conciseness, the test cases (a) will be referred to as *A623K, B623K, C623K, D623K*, whereas the tests (b) will be called *A633K, B633K, C633K, D633K* hereafter.

The correction factors r_σ, r_J, r_G for the numerical simulations are retrieved from Table 2. Tables B.8, B.9 and C.16 report Wilson temperature and the activation time obtained with these simulations,

---

[2] The values for k_1, k_2 neglecting the last two tests are 0.05794 and 0.9339 respectively.
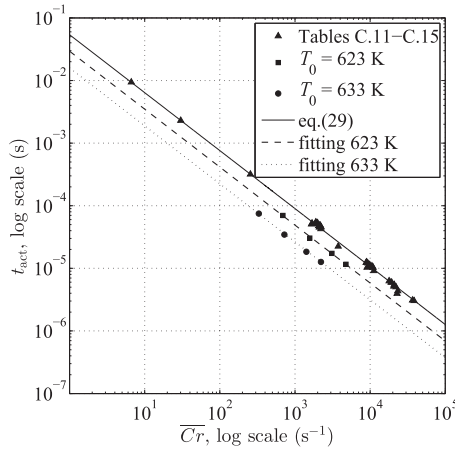
Fig. 12. Activation time as a function of the cooling rate for the simulations in Appendix C, $k_2 = 0.9257$.

Fig. 14. Values of k_1 for nozzle *4B* as a function of $\widetilde{\Delta T}_{cr}$ (obtained from Eq. (30) and Table C.12).

whereas Fig. 12 depicts t_{act} as a function of $\overline{Cr}$.

It is observed that the values t_{act} and $\overline{Cr}$ are correlated by lines (hyperbolas in a linear scale) having very similar slopes. Thus k_2 can be assumed constant and equal to the value in Eq. (30), as the fitting of Eq. (30) gives values of k_2 which are only marginally different.

In order to determine an expression for k_1, the relation in Eq. (30) is inverted. The quantity $Wi\overline{Cr}^{k_2-1}$ for the profiles *2B, 4B, 5B, 6B* is displayed in Figs. 13–16 as a function of the dimensionless temperature difference

$$\widetilde{\Delta T}_{cr} = 1 - \frac{T_{sat}(s_0)}{T_{cr}}. \tag{31}$$

$\widetilde{\Delta T}_{cr}$ is only a function of s_0: for each test case this variable is defined only by the total inlet conditions P_0, T_0.

The values of k_1 can be fitted with an exponential function. Thus, Eq. (29) can be rewritten as

$$t_{act} = k_1(\widetilde{\Delta T}_{cr})\overline{Cr}^{-k_2} = \hat{k}_1\left(1 - \exp\left(-\frac{\widetilde{\Delta T}_{cr}^{k_3}}{\tau_T}\right)\right)\overline{Cr}^{-k_2}. \tag{32}$$

with $k_1 \rightarrow \hat{k}_1(\Delta T \approx 1)$. As Eq. (32) must reduce to Eq. (29) for low $T_{sat}(s_0)$ values, the coefficient $\hat{k}_1$ is taken equal to 0.0539. This results in $k_3 = 1.359$ and $\tau_T = 0.0299$. Consequently, the Wilson number reads

$$Wi = \hat{k}_1\left(1 - \exp\left(-\frac{\widetilde{\Delta T}_{cr}^{k_3}}{\tau_T}\right)\right)\overline{Cr}^{1-k_2}. \tag{33}$$

Fig. 17 reports the function $k_1 = k_1(\widetilde{\Delta T}_{cr})$. Additionally, Fig. 18

reports the Wilson curve according to Eq. (32) for $\overline{Cr}$ values of 1, 100 and 10 000 s⁻¹.

The deviation between the best fit and the values of k_1 for the majority of the cases is less than 10%. However, for a limited number of test cases such value is considerably higher. For instance, three points in Fig. 13 deviate considerably from the exponential trend. These points correspond to nozzle expansions characterized by the lowest $\overline{Cr}$. The same is also observed for nozzle *4B* (Fig. 14): the measurements that are farther from the fitting curve (Tests *21As*, 21Bs*, 21Cs*, 18B* and Test *19Cs**) feature the highest and the lowest cooling rates respectively. A possible explanation for the deviation of these points from the fitting is that k_1 might depend on $\overline{Cr}$.

Fig. 17 shows that the term $\widetilde{\Delta T}_{cr}$ visibly affects the value of k_1 only at high reduced temperatures, namely for $T_{sat}(s_0) > 0.8T_{cr}$. In these conditions, the surface tension starts slowly vanishing, thus reducing the degree of subcooling needed for stable droplets to form. For $T_{sat}(s_0) > 0.9T_{cr}$ the degree of subcooling falls down rapidly, and the thermodynamic state of the condensing vapour is quickly reverted back to equilibrium, even in very fast expansion processes.

By inverting Eq. (32), the cooling rate $\overline{Cr}$ can be rewritten as

$$\overline{Cr} = \left(\frac{k_1(\widetilde{\Delta T}_{cr})}{t_{act}}\right)^{\frac{1}{k_2}}, \tag{34}$$

thus, in terms of activation time, the Wilson number becomes

$$Wi = \overline{Cr} \cdot t_{act} = k_1(\widetilde{\Delta T}_{cr})^{\frac{1}{k_2}} \cdot (t_{act})^{1-\frac{1}{k_2}}. \tag{35}$$

Therefore, given a set of total inlet conditions, thus a set of $\widetilde{\Delta T}_{cr}$

Fig. 13. Values of k_1 for nozzle *2B* as a function of $\widetilde{\Delta T}_{cr}$ (obtained from Eq. (30) and Table C.11).

Fig. 15. Values of k_1 for nozzle *5B* as a function of $\widetilde{\Delta T}_{cr}$ (obtained from Eq. (30) and Table C.13).
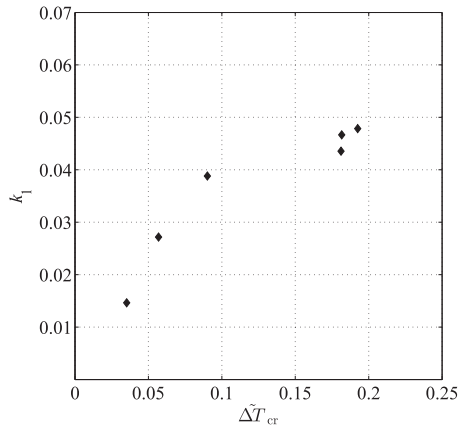
Fig. 16. Values of k_1 for nozzle *6B* as a function of $\widetilde{\Delta T}_{cr}$ (obtained from Eq. (30) and Table C.14).

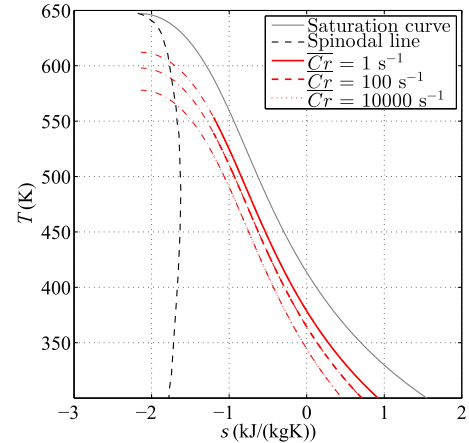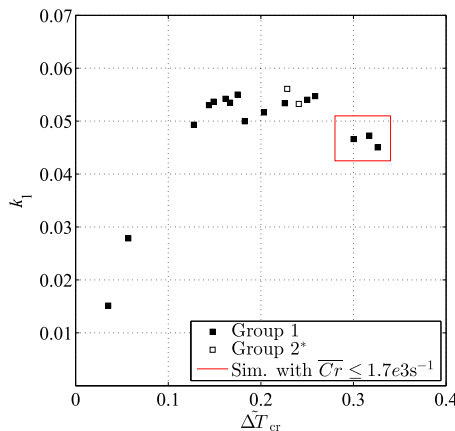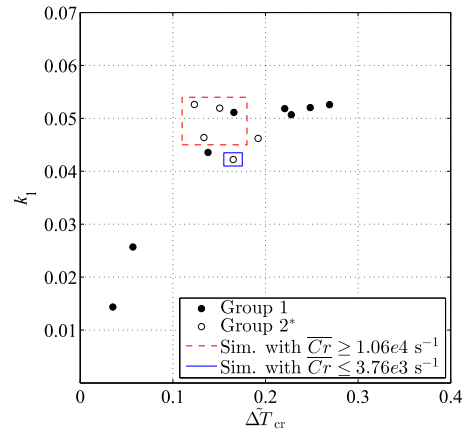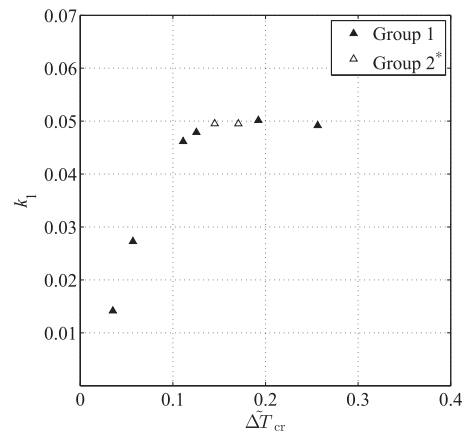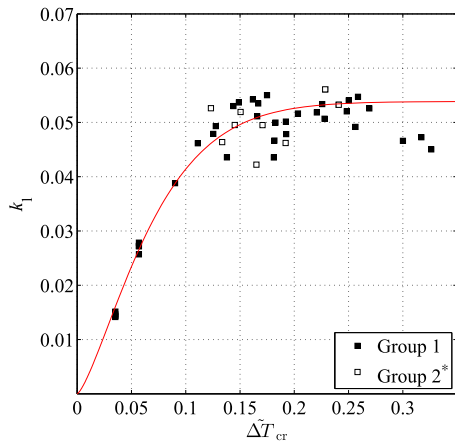**Fig. 17.** Values of k_1 as a function of $\widetilde{\Delta T}_{cr}$ obtained from Eq. (30) and Tables C.11–C.14, fitting function (see Eq. (32)).
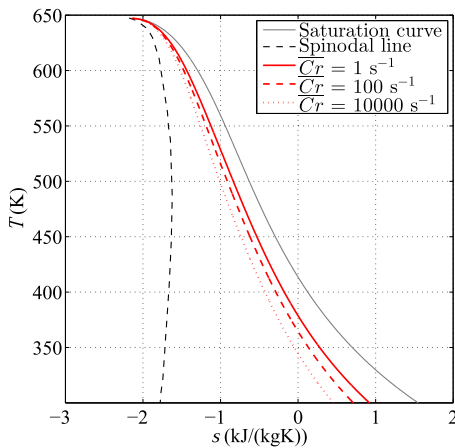
Fig. 18. *T-s* chart reporting saturation curve, spinodal curve and Wilson point as in Eq. (32) for $\overline{Cr} = 1, 100, 10\,000$ s^{-1}.

value, the isentropic subcooling *Wi* becomes only a function of a single variable, i.e., the activation time. Eq. (35) is particularly useful for analysis and design purposes as exemplified in Section 4.

4. Application

4.1. Prediction of the condensation onset in a supersonic nozzle

Eq. (35) for the estimation of the Wilson number *Wi* allows to
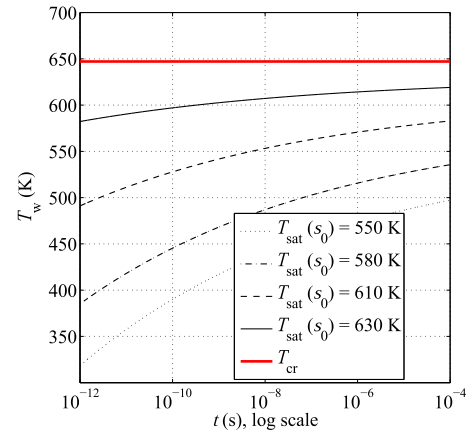
Fig. 19. Wilson cure $T_w(t)$ as a function of the time t_{act}, $T_{sat}(s_0)$ = 550 K, 580 K, 610 K, 630 K.

interpret T_w as a time-dependent function, i.e., $T_w(t)$. Fig. 19 displays $T_w(t)$ for $T_{sat}(s_0)$ = 550 K, 580 K, 610 K, 630 K, corresponding to $\widetilde{\Delta T}_{cr}$ = 0.15, 0.10, 0.06, 0.03 respectively. In order to determine the onset of condensation for an arbitrary expansion process, the following procedure, involving the use of plotted information, is proposed:

1. the curve $T_w(t)$ is drawn for a specified $T_{sat}(s_0)$ in a *T-t* chart;
2. a single-phase simulation allowing for metastable conditions is carried out;
3. the temperature profile along the expansion is displayed in the same *T-t* chart. From the definition of t_{act}, at the time $t = 0$ s the fluid is in saturated conditions, i.e., $T(0) = T_{sat}(s_0)$;
4. stable condensation occurs if the flow reaches the Wilson state. Thus, the nucleation onset corresponds to the intersection point between $T(t)$ and $T_w(t)$.

Once the degree of subcooling is known, the thermodynamic wetness loss can be calculated with the approach proposed in Young (1984).

Fig. 20 reports the curve $T(t)$ for the Barshdorff test-case (Halama and Fort, 2012) along with the correspondent $T_w(t)$. $T_{sat}(s_0)$ is approximately equal to 361 K.

Table 4 shows the Wilson point predictions obtained for four different test-cases reported in Refs. Bakhtar and Zidi (1989) and Halama and Fort (2012). With reference to the tests *B* and *S1*, the deviation between the predicted and the experimental P_w values is less than 2%, whereas for the test *L2* the difference is more pronounced, i.e., approximately 16%. On average, the computational cost of each test
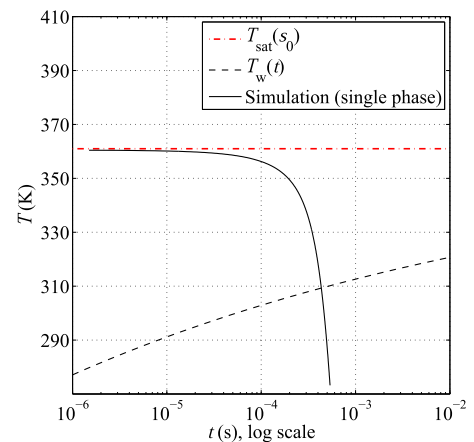
Fig. 20. Temperature profile for the Barshdorff test case (Halama and Fort, 2012) and Wilson point as a function of the time, $T_{sat}(s_0) \simeq 361$ K.

Table 4
Validation of Eq. (32) with four steam supersonic expansions from Refs. Bakhtar and Zidi (1989) and Halama and Fort (2012). Comparison between the experimental Wilson pressure $P_{w, exp}$ and the value predicted by using the proposed semi-analytical method.

Barshdorff (Halama and Fort, 2012)

	P_0	T_0	$T_{sat}(s_0)$	$P_{w, exp}$	t_{act}	$\overline{Cr}$	P_w	Dev.%
B	0.784 bar	373.2 K	361.0 K	0.370 bar	4.33e−4 s	173 s^{-1}	0.366 bar	−1.1

Bakhtar and Zidi (1989)

	P_0	T_0	$T_{sat}(s_0)$	$P_{w, exp}$ ($\pm$ 0.14 bar)	t_{act}	$\overline{Cr}$	P_w	Dev.%
S1	32.0 bar	535.0 K	491.9 K	13.50 bar	5.03e−5 s	1865 s^{-1}	13.71 bar	+1.6
M2	32.0 bar	531.0 K	494.7 K	13.76 bar	4.82e−5 s	1952 s^{-1}	14.49 bar	+5.3
L2	32.0 bar	544.7 K	485.6 K	10.08 bar	3.02e−5 s	3236 s^{-1}	11.70 bar	+16.0
	31.86 bar	546.7 K	484.0 K	10.08 bar	2.93e−5 s	3369 s^{-1}	11.24 bar	+11.5

Fig. 21. Examples of (a) condensation inside the nozzle, (b) condensation at the nozzle outlet and (c) no condensation, $T_{sat}(s_0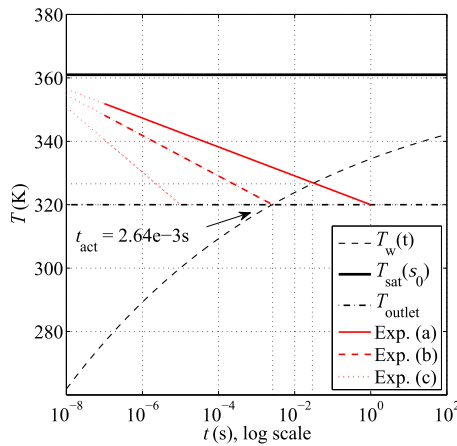) \simeq 361$ K (from Halama and Fort (2012)). Due to the log scale adopted, for the sake of clarity the expansions are displayed starting from $t = 10^{-9}$ s instead of 0 s.

case, if the domain is discretized with 1000 cells, is of the order of five minutes on a single processor Intel(R) Core(TM) i7-4600U CPU @ 2.10GHz.

In order to assess the effect of experimental uncertainty, which is $\pm$ 2 K on T_0 and $\pm$ 0.14 bar on P_0, another simulation was performed with a value of P_0 decreased of the uncertainty interval and a value of T_0 increased by the uncertainty interval. This is done in order to obtain a simulation result that is closer to the measurement, with input conditions that are still within the experimental uncertainty (Table 4). The deviation in this case is 11.5%. Deviations are arguably due to the dependence of k_1 from $\overline{Cr}$, see Eq. (32). The L2 test features a value of $\overline{Cr}$, see Fig. 13.

Overall, the accuracy of the proposed method is of the same order of that of more complex models (Bakhtar and Zidi, 1990) and better if compared to other numerical models based on the method of moments documented in the literature. As an example, the model used in the simulations of the L2 test case discussed in Ref. Giordano et al. (2010) leads to a value of P_w that is 40 % different from the measured value.

From the results in Table 4, it can be seen that the higher is the cooling rate, the higher is the difference between measured and estimated P_w values. This can be ascribed to the assumptions affecting k_1, k_2. Additional measurements are required to fully work out the dependence of k_1 and k_2 on the cooling rate, especially for values in excess of 2e3 s^{-1} (i.e. 1.3e6 K/s).

4.2. Design of converging-diverging nozzles

The proposed semi-analytical model can be exploited for design purposes. For example, consider the design of an adapted nozzle free of condensation, thus unaffected by the associated thermodynamic wetness losses. The specified operating conditions are P_0, T_0 and static back-pressure.

Fig. 21 shows three expansions in the T-t chart characterized by $\overline{Cr}$ values of (a) 0.06 s^{-1}, (b) 24 s^{-1}, and (c) 6 000 s^{-1}. $T_{sat}(s_0)$ is 361 K, the same as that in the Barshdorff test case, whereas a nozzle static back-pressure of 0.42 bar is arbitrarily imposed at the outlet boundary, corresponding to a static back temperature of 320 K assuming isentropic expansion.

As anticipated, the onset of stable condensation is located at the intersection of the curves $T_w(t)$ and $T(t)$. For instance, the Wilson temperature for expansion (a) is approximately 326 K, whereas in expansion (b) condensation will occur only in correspondence of the nozzle outlet section. In expansion (c) the Wilson temperature is well below the outlet temperature of the nozzle, thus it can be argued that condensation does not occur.

In essence, homogeneous condensation is not triggered if the residence time of subcooled steam within the nozzle is lower than the activation time corresponding to a characteristic $\overline{Cr}$, cf. expansion (b) and (c). Therefore, given the total inlet conditions and the outlet back-pressure leading to an expansion process below the saturation conditions, the curve $T_w(t)$ provides the minimum cooling rate $\overline{Cr}$ required to avoid the formation of condensing fog inside the channel. $\overline{Cr}$ can be used as input or constraint for a design of condensation-free supersonic nozzles expanding steam.

Note that the cooling rate is directly related to the nozzle length L, as the activation time t_{act} can be defined for a 1D test case as

$$t_{act} = \int_{x(T_{sat}(s_0))}^{x(T_w)} \frac{dx}{v}, \tag{36}$$

where x is the coordinate along the nozzle axis and v is the velocity of the flow. By stretching the nozzle geometry along the coordinate x, one can modify the final cooling rate. As an example, $\overline{Cr}$ can be doubled by reducing the total length L of the nozzle by a factor 2.

Suppose that the method of characteristics is used to design the divergent section of a nozzle profile (Guardone et al., 2013). In this case, the parameter L is calculated as a function of (i) the flow conditions and (ii) the throat curvature radius r_t. Eq. (35) can provide the minimum cooling rate required to avoid condensation, thus, a reference value L that can be used to determine a suitable r_t value for a revised nozzle design.

5. Conclusions

A new semi-analytical model for the estimation of the Wilson point in steam supersonic expansions has been developed and validated by comparison with experimental information. The goal of the modelling effort was two-fold: first, identifying the most significant flow parameters affecting the condensation onset and quantifying the impact of such parameters on the Wilson point; secondly, the establishment of a simplified procedure for the prediction of condensation in nozzle flows suitable for analysis and design.

In order to account for the influence of $\overline{Cr}$ and $T_{sat}(s_0)$, the Wilson point definition was reformulated in such a way that T_w could be obtained in terms of the Wilson number $Wi(t)$, a new dimensionless and time-dependent quantity. It was therefore found that:

1. for the range of cooling rates observed in steam nozzle expansions documented in Gyarmathy (2005) (order of $10^6 - 10^7$ K/s), the Wilson number Wi weakly depends on $\overline{Cr}$;
2. the effect of T_{sat} on the location of the Wilson point becomes significant for $T_{sat}(s_0) > 0.8 T_{cr}$. For $T_{sat}(s_0) > 0.9 T_{cr}$, the surface tension rapidly vanishes and stable condensation is promoted, regardless of the cooling rate of the expansion.

Furthermore, the Wilson temperature $T_w(t)$ can be used to predict the onset of condensation without the need of performing demanding two-phase simulations. The application of Eq. (35) in four different test cases revealed that the accuracy of the obtained predictions is of the same order of those estimated with more complex models available in the literature. Once the degree of subcooling is known, associated thermodynamic wetness losses can be estimated a priori with available models (Young, 1984).

Finally, the model can also be applied in the design of condensation-free nozzles, as it allows to retrieve the minimum cooling rate needed to prevent inception of stable condensation.

The proposed approach, currently restricted to steam flow, can be extended to arbitrary fluids, provided that experimental data are available to calibrate the numerical model. This is the focus of ongoing and future work.

Appendix A. Determination of r_σ, r_J, r_G

This table reports the steps for the empirical determination of r_σ, r_J, r_G for the test case No. *21As** (Gyarmathy, 2005). To correctly locate the Wilson pressure along the simulation, the min and max values for Pw were taken as the limits of the expansion portion with a visible change in the pressure derivative over the nozzle coordinate.

Table A1
Determination of r_σ, r_J, r_G: example on test case No.21As* in Gyarmathy (2005).

Simulation results								
Corrections			**P_w (bar)**		**$\overline{R}_w$ (m x1e-8)**		**N_w (1/kg x1e16)**	
r_σ	r_J	r_G	from	to	from	to	from	to
1.40	0.29	0.23	54.7	51.4	0.15	0.42	7.35	14.63
1.41	0.29	0.23	54.5	50.9	0.15	0.43	5.51	13.87
1.43	0.29	0.23	53.4	49.0	0.16	0.47	4.91	12.44
1.45	0.29	0.23	52.1	47.8	0.18	0.49	5.61	11.11
1.48	0.29	0.23	50.3	46.5	0.19	0.50	4.82	9.31
1.48	0.26	0.23	50.3	45.8	0.20	0.50	4.70	9.18
1.48	0.26	0.20	49.9	45.3	0.18	0.49	6.23	11.75
1.48	0.23	0.20	49.6	45.8	0.19	0.47	6.97	11.55
1.49	0.23	0.20	49.2	45.0	0.19	0.49	5.89	10.86
1.49	0.23	0.23	50.2	44.4	0.19	0.55	2.80	8.51
1.49	0.26	0.23	49.7	44.8	0.20	0.54	4.20	8.64

Experimental pressure: $P_w = 47.20$ bar
Experimental average radius: $5.86e - 8$ m $\leq \overline{R}_w \leq 5.918e - 8$ m
Experimental droplet number: $6.15e16$ 1/kg $\leq N_w \leq 6.26e16$ 1/kg

Appendix B. Simulation results

The following tables report the pressure and temperature P_w, T_w, the average radius $\overline{R}_w$ and the number of drops N_w per unit of total mass in correspondence with the Wilson point obtained from the simulations. The final three columns reports the values of r_σ, r_J, r_G. In particular, r_σ is factor with the main influence on the condensation onset, and visible deviations are present for using a step of ± 0.01. After the surface tension is set, r_J and r_G are changed to match the experimental average radius and number of droplets at the Wilson point. As the effect of these two parameters is not as significant as for r_σ, their value can be determined with a lower accuracy. Due to the uncertainties related to the Wilson point location, for every property the tables report a minimum and a maximum value, as in Gyarmathy (2005).

The analysis in the paper considers average pressures and temperatures in such intervals.

Table B1
Properties at Wilson point and corrections adopted for the simulations with nozzle *2B*.

Test No.	Nozzle	P_0(bar)	T_0 (K)	P_w (bar)		T_w (K)		$\bar{R}_w$ (x1e-8 m)		N_w (x1e16 1/kg)		r_σ	r_J	r_G
				from	to	from	to	from	to	from	to			
13B	2B	20.82	574.28	3.97	3.60	383.28	405.60	1.70	6.02	1.01	3.46	1.06	0.89	0.56
13C	2B	20.83	562.45	4.52	4.07	387.06	409.75	1.95	6.84	0.79	2.49	1.09	0.89	0.53
13D	2B	20.82	541.2	6.03	5.57	398.90	419.55	2.49	8.09	0.59	1.36	1.1	0.89	0.56
*14B**	2B	61.48	631.63	13.35	11.58	429.35	447.83	2.75	9.26	0.32	1.23	1.24	0.59	0.32
15C	2B	96.78	647.69	28.47	25.34	470.23	485.60	3.35	10.24	0.43	0.99	1.31	0.41	0.29
*34A**	2B	50.04	584.26	16.73	14.66	441.51	455.97	2.63	9.36	0.08	1.07	1.26	0.47	0.29
35A	2B	79.46	660.01	15.00	13.34	432.65	451.70	3.18	8.73	0.96	1.46	1.28	0.47	0.26
35B	2B	79.46	634.97	21.79	19.65	454.78	471.00	3.25	9.52	0.56	1.09	1.28	0.47	0.29
36C	2B	106.92	645.71	34.79	31.59	479.19	491.57	3.73	10.68	0.29	0.80	1.4	0.35	0.26
37B	2B	138.30	674.25	43.42	37.81	494.02	506.53	3.01	10.09	0.20	1.28	1.43	0.29	0.2
38B	2B	50.04	619.28	10.25	9.00	416.32	437.05	2.28	7.42	0.79	2.32	1.22	0.5	0.26
38B'	2B	50.04	609.69	11.54	10.34	421.88	442.18	2.57	7.57	1.18	2.09	1.22	0.5	0.26
39D	2B	89.27	619.75	32.91	31.17	476.16	488.25	4.20	9.85	0.56	0.80	1.38	0.35	0.26
40C	2B	108.88	660.44	29.85	27.00	470.03	484.01	3.60	10.18	0.42	0.93	1.37	0.38	0.26
40D	2B	108.88	637.36	40.26	37.75	493.22	503.15	3.89	10.02	0.55	0.93	1.42	0.29	0.23
40E	2B	108.88	619.08	53.06	49.86	508.82	518.82	3.04	9.46	0.30	1.11	1.45	0.26	0.17

The comparison with Gyarmathy (2005) *is made with a nominal value instead of an uncertainty interval for one of the properties reported*

Table B2
Properties at Wilson point and corrections adopted for the simulations with nozzles *4B, 5B, 6B*.

Test No.	Nozzle	P_0(bar)	T_0 (K)	P_w (bar)		T_w (K)		$\bar{R}_w$ (x1e-8 m)		N_w (x1e16 1/kg)		r_σ	r_J	r_G
				from	to	from	to	from	to	from	to			
18B	4B	100.70	638.45	27.71	29.67	463.80	476.80	2.49	4.41	9.90	10.35	1.35	0.35	0.26
18C	4B	100.70	615.2	42.48	43.91	493.10	503.20	2.10	4.11	10.52	10.69	1.4	0.29	0.23
19A	4B	61.47	610.25	16.23	14.45	435.72	453.42	1.72	4.33	9.93	12.57	1.25	0.41	0.38
*19B**	4B	61.47	583.4	24.34	22.87	461.47	476.64	2.49	4.85	7.60	7.78	1.26	0.47	0.41
*19Cs**	4B	61.47	560.55	37.31	34.42	487.12	488.80	1.86	4.10	4.75	3.57	1.26	0.47	0.41
20A	4B	40.43	575.18	11.08	10.19	417.01	437.14	1.71	4.05	10.82	12.87	1.22	0.5	0.44
20B	4B	40.43	555.72	15.04	14.07	432.35	448.47	1.57	4.15	6.14	10.15	1.23	0.47	0.41
20D	4B	40.43	598.1	8.09	7.44	402.28	423.90	1.50	3.64	14.20	17.48	1.2	0.56	0.5
*21As**	4B	132.10	648.2	50.16	44.39	497.75	510.91	1.86	5.50	2.80	8.51	1.49	0.26	0.23
*21Bs**	4B	132.10	657	47.79	42.93	499.19	511.93	1.99	5.87	2.48	6.26	1.41	0.29	0.35
*21Cs**	4B	132.10	671.5	38.04	33.82	481.67	493.28	1.72	5.07	2.23	8.48	1.41	0.35	0.29
*23A**	5B	100.70	662.6	22.61	19.77	451.12	472.76	1.43	3.85	16.21	22.35	1.3	0.5	0.38
23B	5B	100.70	641.74	29.20	26.80	465.36	479.19	2.02	4.27	11.01	13.19	1.35	0.35	0.44
23C	5B	100.70	620.55	39.25	36.15	483.26	493.28	2.02	4.44	8.08	10.76	1.4	0.29	0.41
*24As**	5B	41.00	584	9.96	8.99	411.24	434.45	1.12	3.01	7.73	34.74	1.2	0.71	0.53
*25As**	5B	148.10	668.6	49.94	43.34	498.68	511.84	1.85	5.07	6.50	12.00	1.45	0.23	0.38
*25Bs**	5B	148.10	656.7	58.35	52.49	509.82	519.87	2.15	5.36	5.40	9.04	1.49	0.2	0.41
26C	6B	61.47	573.93	27.90	25.18	466.68	471.83	1.38	0.34	6.65	15.70	1.26	0.41	0.74
27A	6B	100.70	662.93	22.25	19.74	450.83	470.49	1.70	4.11	14.18	17.10	1.29	0.47	0.8
28Ao	6B	149.74	642.49	77.52	70.33	535.96	533.67	2.07	4.95	2.17	7.82	1.51	0.26	0.71
29Ao	6B	81.09	617.3	26.33	23.08	460.69	475.90	1.32	3.63	12.78	22.97	1.29	0.47	0.71

The comparison with Gyarmathy (2005) *is made with a nominal value instead of an uncertainty interval for one of the properties reported*

Table B3
Properties at Wilson point and corrections adopted for the simulations at 623 K.

Test No.	Nozzle	P_0(bar)	T_0 (K)	P_w (bar)		T_w (K)		$\bar{R}_w$ (x1e-8 m)		N_w (x1e16 1/kg)		r_σ	r_J	r_G
				from	to	from	to	from	to	from	to			
A623	2B	154.19	623	118.51	113.58	580.81	578.38	4.68	7.32	1.91	2.27	1.55	0.17	0.21
B623	4B	154.19	623	115.90	111.83	577.63	575.03	3.19	4.53	6.69	8.21	1.55	0.17	0.25
C623	5B	154.19	623	114.59	106.56	576.10	570.85	3.29	5.14	6.86	8.30	1.55	0.17	0.4
D623	6B	154.19	623	116.17	107.10	571.06	570.80	3.06	5.35	3.65	6.56	1.55	0.17	0.71

Table B4
Properties at Wilson point and corrections adopted for the simulations at 633 K.

Test No.	Nozzle	P_0(bar)	T_0 (K)	P_w (bar)		T_w (K)		$\bar{R}_w$ (x1e-8 m)		N_w (x1e16 1/kg)		r_σ	r_J	r_G
				from	to	from	to	from	to	from	to			
A633	2B	179.21	633	158.67	149.59	613.44	605.40	2.05	5.56	0.00	4.61	1.57	0.15	0.21
B633	4B	179.21	633	5526.23	151.61	611.71	606.94	1.54	3.01	0.57	14.99	1.57	0.15	0.25
C633	5B	179.21	633	156.64	146.41	611.52	605.52	1.54	3.92	0.06	13.32	1.57	0.15	0.4
D633	6B	179.21	633	157.10	145.55	612.01	605.10	1.63	4.43	0.02	10.48	1.57	0.15	0.7

Table B5
Properties at Wilson point and corrections adopted for the simulations with the Moore nozzle (Azzini et al., 2016).

Test No.	Nozzle	P_0(bar)	T_0 (K)	P_w (bar)		T_w (K)		$\bar{R}_w$ (x1e-8 m)		N_w (x1e16 1/kg)		r_σ	r_J	r_G
				from	to	from	to	from	to	from	to			
M	1	0.25	358	0.094	0.098	283.54	311.50	1.61	4.52	4.58	5.64	1	1	1
Mx10	10	0.25	358	0.087	0.088	285.51	293.59	7.06	16.97	1.66E−02	2.90E−02	1	1	1
Mx25	25	0.25	358	0.092	0.091	288.33	293.79	12.57	32.99	5.42E−04	2.61E−02	1	1	1
Mx1e5	1e5	0.28	380.20	0.102	0.101	297.88	301.58	3.25e3	6.80e3	2.66e−10	3.10e−10	1	1	1
Mx1e10	1e10	0.28	380.20	0.151	0.146	327.10	329.55	5.62E+05	1.88E+06	4.10E−20	1.39E−17	1	1	1

Appendix C. Activation time and cooling rate data

The following tables show i) the dimensionless saturation temperature $T_{sat}(s_0)$ and ii) a second point along the expansion at time $t_{subcooled} < t_{act}$ characterized by temperature $T_{subcooled}$. These informations are used to evaluate the average cooling rate $\overline{Cr}$. The last column reports the activation time t_{act}.

Table C1
Cooling rate and activation time for nozzle 2B.

Test No.	$T_{sat}(s_0)/T_{cr}$	$t_{subcooled}$ (s)	$T_{subcooled}/T_{cr}$	$\overline{Cr}$ (s^{-1})	t_{act} (s)
13B	0.674	5.01E−05	0.591	1.66E+03	5.07E−05
13C	0.683	5.07E−05	0.598	1.69E+03	5.25E−05
13D	0.700	4.90E−05	0.617	1.70E+03	5.13E−05
14B*	0.759	5.01E−05	0.662	1.94E+03	5.20E−05
15C	0.817	4.31E−05	0.727	2.10E+03	4.53E−05
34A	0.774	5.04E−05	0.678	1.91E+03	5.29E−05
35A*	0.772	5.13E−05	0.669	2.00E+03	5.32E−05
35B	0.797	4.49E−05	0.704	2.06E+03	4.77E−05
36C	0.838	4.54E−05	0.741	2.15E+03	4.82E−05
37B	0.856	4.26E−05	0.761	2.23E+03	4.55E−05
38B	0.741	5.13E−05	0.644	1.89E+03	5.46E−05
38B'	0.750	4.98E−05	0.655	1.91E+03	5.36E−05
39D	0.833	4.44E−05	0.739	2.11E+03	4.83E−05
40C	0.825	4.41E−05	0.730	2.17E+03	4.85E−05
40D	0.851	4.26E−05	0.758	2.18E+03	4.71E−05
40E	0.872	3.78E−05	0.789	2.21E+03	4.27E−05

Table C2
Cooling rate and activation time for nozzle 4B.

Test No.	$T_{sat}(s_0)/T_{cr}$	$t_{subcooled}$ (s)	$T_{subcooled}/T_{cr}$	$\overline{Cr}$ (s^{-1})	t_{act} (s)
18B	0.834	9.13E−06	0.735	1.09E+04	1.03E−05
18C	0.862	8.86E−06	0.781	9.09E+03	1.03E−05
19A	0.779	1.03E−05	0.677	9.86E+03	1.14E−05
19B*	0.808	9.55E−06	0.718	9.40E+03	1.06E−05
19Cs*	0.835	2.05E−05	0.758	3.76E+03	2.25E−05
20A	0.752	1.13E−05	0.647	9.28E+03	1.21E−05
20B	0.772	1.12E−05	0.673	8.85E+03	1.23E−05
20D	0.731	1.20E−05	0.623	8.99E+03	1.26E−05
21As*	0.877	1.05E−05	0.766	1.06E+04	1.09E−05
21Bs*	0.866	8.57E−06	0.771	1.12E+04	9.12E−06
21Cs*	0.849	9.85E−06	0.742	1.09E+04	1.04E−05

Table C3
Cooling rate and activation time for nozzle 5B.

Test No.	$T_{sat}(s_0)/T_{cr}$	$t_{subcooled}$ (s)	$T_{subcooled}/T_{cr}$	$\overline{Cr}$ (s^{-1})	t_{act} (s)
23A*	0.808	5.70E−06	0.697	1.94E+04	5.95E−06
23B	0.829	5.20E−06	0.721	2.09E+04	5.48E−06
23C	0.855	5.66E−06	0.747	1.90E+04	5.99E−06
24As*	0.744	5.95E−06	0.637	1.79E+04	6.28E−06
25As*	0.875	4.73E−06	0.770	2.21E+04	5.03E−06
25Bs*	0.889	4.92E−06	0.787	2.07E+04	5.17E−06

Table C4
Cooling rate and activation time for nozzle 6B.

Test No.	$T_{sat}(s_0)/T_{cr}$	$t_{subcooled}$ (s)	$T_{subcooled}/T_{cr}$	$\overline{Cr}$ (s^{-1})	t_{act} (s)
26C	0.819	4.13E−06	0.722	2.33E+04	4.36E−06
27A	0.807	2.84E−06	0.698	3.85E+04	3.03E−06
28Ao	0.910	3.72E−06	0.825	2.28E+04	3.96E−06
29Ao	0.818	2.91E−06	0.712	3.66E+04	3.09E−06

Table C5
Cooling rate and activation time, simulations with Moore nozzle.

Test No.	$T_{sat}(s_0)/T_{cr}$	$t_{subcooled}$ (s)	$T_{subcooled}/T_{cr}$	$\overline{Cr}$ (s^{-1})	t_{act} (s)
M	0.506	2.99E−04	0.429	2.55E+02	3.19E−04
Mx10	0.506	2.06E−03	0.443	3.02E+01	2.30E−03
Mx25	0.506	8.53E−03	0.449	6.63E+00	9.42E−03
Mx1e5	0.506	1.19E+01	0.482	2.01E−03	1.29E+01
Mx1e10	0.506	6.06E+05	0.491	2.38E−08	6.90E+05

Table C6
Cooling rate and activation time, simulations at T_0 equal to 623 K and 633 K.

Test No.	$T_{sat}(s_0)/T_{cr}$	$t_{subcooled}$ (s)	$T_{subcooled}/T_{cr}$	$\overline{Cr}$ (s^{-1})	t_{act} (s)
A623K	0.943	6.05E−05	0.901	6.91E+02	6.99E−05
B623K	0.943	3.04E−05	0.895	1.57E+03	3.04E−05
C623K	0.943	1.73E−05	0.889	3.10E+03	1.73E−05
D623K	0.943	1.16E−05	0.888	4.78E+03	1.16E−05
A633K	0.965	7.49E−05	0.940	3.30E+02	7.49E−05
B633K	0.965	3.46E−05	0.940	7.23E+02	3.46E−05
C633K	0.965	1.84E−05	0.939	1.42E+03	1.84E−05
D633K	0.965	1.27E−05	0.937	2.21E+03	1.27E−05

References

Azzini, L., Pini, M., 2017. Numerical investigation of high pressure condensing flows in supersonic nozzles. J. Phys. Conf. Ser., vol. 821.

Azzini, L., Van Der Stelt, T.P., Pini, M., 2016. Numerical investigation of metastable condensing flows with an implicit upwind method. ECCOMAS Congress 2016 - Proceedings of the 7th European Congress on Computational Methods in Applied Sciences and Engineering. Vol. 4. pp. 7165–7181.

Bakhtar, F., Young, J.B., White, A.J., Simpson, D.A., 2005. Classical nucleation theory and its application to condensing steam flow calculations. Proc. Inst. Mech. Eng. Part C J. Mech. Eng. Sci. 219 (12), 1315–1333.

Bakhtar, F., Zidi, K., 1989. Nucleation phenomena in flowing high-pressure steam: experimental results. ARCHIVE Proc. Inst. Mech. Eng. Part A J. Power Eng. 203 (31), 195–200. 1989 (vol 203).

Bakhtar, F., Zidi, K., 1990. Nucleation phenomena in flowing high-pressure steam part 2: theoretical analysis. ARCHIVE Proc. Inst. Mech. Eng. Part A J. Power Energy 204 (41), 233–242. 1990–1996 (vols 204–210).

Bier, K., Ehrler, F., Theis, G., 1990. Spontaneous condensation in stationary nozzle flow of carbon dioxide in a wide range of density. Adiabatic Waves in Liquid–Vapour Systems. Springer Science + Business Media, pp. 129–141.

Bruno, T.J., Ely, J.F., 1991. Supercritical Fluid Technology. CRC Press, pp. 451–478.

Colonna, P., der Stelt, T.V., 2004. Fluidprop: A Program for the Estimation of Thermo Physical Properties of Fluids. Delft University of Technology, The Netherlands. http://www.FluidProp.com.

Ding, H., Wang, C., Wang, G., Chen, C., 2015. Analytic equations for the wilson point in high-pressure steam flow through a nozzle. Int. J. Heat Mass Transfer 91, 961–968.

Dobbins, R.A., 1983. A theory of the wilson line for steam at low pressures. J. Fluids Eng. 105 (4), 414.

Dykas, S., Wróblewski, W., 2012. Numerical modelling of steam condensing flow in low and high-pressure nozzles. Int. J. Heat Mass Transfer 55 (21–22), 6191–6199. Elsevier BV.

Gerber, A., Kermani, M., 2004. A pressure based Eulerian–Eulerian multi-phase model for non-equilibrium condensation in transonic steam flow. Int. J. Heat Mass Transfer 47, 2217–2231. Elsevier BV.

Giordano, M., Hercus, S., Cinnella, P., 2010. Effects of modelling uncertainties in condensing wet-steam flows through supersonic nozzles. V European Conference on Computational Fluid Dynamics ECCOMAS, Lisbon, Portugal.

Guardone, A., Spinelli, A., Dossena, V., 2013. Influence of molecular complexity on nozzle design for an organic vapour wind tunnel. J. Eng. Gas Turbine Power 135 (4), 042307.

Guo, T., Sumner, W.J., Hofer, D.C., 2007. Development of highly efficient nuclear HP steam turbines using physics based moisture loss models. Volume 6: Turbo Expo 2007, Parts A and B. ASME International.

Gyarmathy, G., 1962. Grundlagen einer Theorie der Naßdampfturbine. Phd thesis. Eidgenössischen technischen hochschule, Zurich.

Gyarmathy, G., 1963. Zur wachstumsgeschwindigkeit kleiner flüssigkeitstropfen in einer übersättigten atmosphäre. J. Appl. Math. Phys. (ZAMP) 14 (3), 280–293.

Gyarmathy, G., 2005. Nucleation of steam in high-pressure nozzle experiments. Proc. Inst. Mech. Eng. Part A J. Power Energy 219 (6), 511–521.

Halama, J., Fort, J., 2012. Numerical simulation of steam condensation in a nozzle. EPJ Web of Conferences. 25 EDP Sciences.

Hamidi, S., Kermani, M., 2015. Numerical study of non-equilibrium condensation and shock waves in transonic moist-air and steam flows. Aerosp. Sci. Technol. 46, 188–196.

Huang, L., Young, J.B., 1996. An analytical solution for the wilson point in

homogeneously nucleating flows. Proc. R. Soc. A Math. Phys. Eng. Sci. 452 (1949), 1459–1473.

IJzermans, R.H.A., Hagmeijer, R., van Langen, P.J., 2007. Accumulation of heavy particles around a helical vortex filament. Phys. Fluids 19 (10).

Kulmala, M., Vehkamäki, H., Petäjä, T., Maso, M.D., Lauri, A., Kerminen, V.-M., Birmili, W., McMurry, P., 2004. Formation and growth rates of ultrafine atmospheric particles: a review of observations. J. Aerosol Sci. 35 (2), 143–176.

Lai, D.S., Kadambi, J.R., 1990. Monodisperse droplet generation by spontaneous condensation of steam flow in nozzles. Part. Sci. Technol. 8 (1–2), 55–75. Informa UK Limited.

Leipertz, A., Fröba, A.P., 2008. Improvement of condensation heat transfer by surface modifications. Heat Transfer Eng. 29 (4), 343–356.

McDonald, J.E., 1974. Homogeneous nucleation of vapour condensation i. thermodynamic aspects. Homogeneous Nucleation Theory. Elsevier BV, pp. 225–237.

Moore, M., Walters, P., Crane, R., Davidson, B., 1973. Predicting the fog-drop size in wet-steam turbines. Proceedings of the IMechE Conference on Heat and Fluid Flow in Steam and Gas Turbine Plant. pp. 101–109.

Put, F., 2003. Numerical simulation of condensation in transonic flows. Ph.D. thesis.

University of Twente, Enschede, The Netherlands.

Ryzhov, Y.A., Pirumov, U.G., Gorbunov, V.N., 1989. Nonequilibrium Condensation in High-Speed Gas Flows. New York : Gordon and Breach Science Publishers.

Sheeran, P.S., Matsuura, N., Borden, M.A., Williams, R., Matsunaga, T.O., Burns, P.N., Dayton, P.A., 2016. Methods of generating sub-micron phase-shift perfluorocarbon droplets for applications in medical ultrasonography. IEEE Trans. Ultrason. Ferroelectr. Freq. Control.

van der Stelt, T.P., Nannan, N.R., Colonna, P., 2012. The iPRSV equation of state. Fluid Phase Equilib. 330, 24–35.

Vargaftik, N.B., Volkov, B.N., Voljak, L.D., 1983. International tables of the surface tension of water. J. Phys. Chem. Ref. Data 12 (3). AIP Publishing.

Wagner, W., et al., 2008. IAPWS Industrial Formulation 1997 for the Thermodynamic Properties of Water and Steam. Springer Science + Business Media, pp. 7–150.

White, A.J., 2003. A comparison of modelling methods for polydispersed wet-steam flow. Int. J. Numer. Methods Eng. 57, 819–834. Wiley-Blackwell.

Yellott, J., 1934. Supersaturated steam. Engineering 137.

Young, J., 1984. Semi-analytical techniques for investigating thermal non-equilibrium effects in wet steam turbines. Int. J. Heat Fluid Flow 5 (2), 81–91.